ISET Journal of Earthquake Technology, Paper No. 508, Vol. 47, No. 1, March 2010, pp. 25–46

USE OF STRONG-MOTION DATA FOR FREQUENCY-DEPENDENT SHEAR WAVE ATTENUATION STUDIES IN THE PITHORAGARH REGION OF KUMAON HIMALAYA

A. Joshi*, M. Mohanty**, A.R. Bansal***, V.P. Dimri*** and R.K. Chadha***

*Department of Earth Sciences, Indian Institute of Technology Roorkee, Roorkee-247667
**SERC Division, Department of Science and Technology, Government of India, New Delhi-110016
***National Geophysical Research Institute, Hyderabad-500606

ABSTRACT

The Pithoragarh district in the state of Uttarakhand, India lies in the border region of India and Nepal and falls in the seismically active zone of Kumaon Himalaya. A local network of eight strong-motion accelerographs has been installed in this region since March 2006. The installed strong-motion instruments have recorded several events in this region. These events are located using HYPO71 and the processed digital data is used for obtaining the frequency-dependent shear wave attenuation. This paper presents a method of finding $Q_\beta(f)$ from the strong-motion data, which is based on the modified method of Joshi (2006). Based on the availability of data, hypocentral parameters, and clear S-phases, a total of 27 strong-motion records from six stations are used in this work. By using the inversion algorithm developed in this work, an average relation in the form, $Q_\beta(f) = 30 f^{1.45}$, is obtained for the Pithoragarh region of Kumaon Himalaya.

KEYWORDS: Strong Motion, Attenuation, Inversion, Himalaya

INTRODUCTION

The Kumaon Himalaya is one of the seismically active regions of the world. Most parts of this region fall in the highest seismic hazard zone defined in the seismic zoning map of India. During the last 100 years, this region has been visited by 14 earthquakes of magnitudes greater than 6.0. It has been observed that the devastation caused by any earthquake in a region is directly related to the attenuation characteristics of the medium and to the amount of seismic energy released during the earthquake. The attenuation characteristics of the medium control the decay of the seismic energy in the lithosphere, and the source characteristics of the earthquake control the amount of energy released during the earthquake. Seismic energy attenuates differently in different rocks. The attenuation of seismic energy signifies a reduction in the energy caused by the heterogeneity and anelasticity in the earth.

The attenuation of seismic energy can be defined by the dimensionless quantity known as quality factor Q. This parameter is used to measure the tendency of material to dissipate energy during deformations. Although different fundamental definitions have been proposed for Q, the common idea has been to consider a ratio of potential energy to the dissipated energy over one period of harmonic deformations (Pelton, 2005). Attenuation is a petrophysical parameter that is sensitive to the lithology and physical properties like pressure, temperature, saturation with fluid, gas, etc. (Toksöz et al., 1979). Therefore, direct estimate of attenuation gives us an idea about the characteristics of the medium. The estimates of Q have been found to be frequency-dependent by several researchers worldwide (Aki and Chouet, 1975; Aki, 1980; Gupta et al., 1995; Mandal et al., 2001). Numerous studies have been done worldwide to understand the attenuation characteristics by estimating Q based on P-waves (i.e., Q_α), S-waves (i.e., Q_β) and coda waves (i.e., Q_c). Very little work has been done, however, in the part of Kumaon and Garhwal Higher Himalaya to estimate the attenuation properties of the medium. Paul et al. (2003) estimated the frequency-dependent coda Q relationship as (92±4.73) $f^{1.0\pm0.023}$ by using the single back scattering model proposed by Aki and Chouet (1975). Based on the study of the aftershock

data of the Chamoli earthquake, Mandal et al. (2001) estimated $Q_c(f)$ as (30±0.8) $f^{1.21\pm0.03}$ for the region surrounding the epicenter of the main shock of the Chamoli earthquake. Gupta et al. (1995) estimated $Q_c(f)$ for the Garhwal Himalaya as 126 $f^{0.95}$ by using seven local earthquakes ($2.4 \leq M_L$; 105 $f^{0.76} \leq 4.9$) recorded at five stations on 1.0-Hz velocity sensors. In all studies related to the estimation of coda $Q_c(f)$ relation for the Himalayan region, the single backscattering model proposed by Aki and Chouet (1975) has been used. Recently, a technique has been developed by Joshi (2006) which uses the S-phase of an accelerogram as input in an inversion algorithm and gives $Q_\beta(f)$ and corner frequency f_c of the input events. In the approach given by Joshi (2006) a two-step inversion algorithm was applied to remove near-site effects in the accelerogram due to the unavailability of sufficient data for site studies. Using this technique, Joshi (2006) has estimated $Q_c(f) = 112\ f^{0.97}$ for the Garhwal Himalaya. In the present work we have used the vertical component of acceleration records, which is supposedly free from the site effects. Due to this reason, the two-step inversion used in the earlier approach is now reduced to a single-step algorithm. Further, in order to obtain a direct estimate of corner frequency, we have included a tree search in the inversion algorithm, which was not present in the earlier approach of Joshi (2006). The data used in this paper is collected from a strong-motion network installed in the Kumaon region.

TECTONICS OF THE REGION

The frequent seismic activity and thrust system present in the Kumaon Himalaya demonstrate the seismotectonic importance of the region. The Kumaon sector manifests strong deformations and reactivation of some of the faults and thrusts during the Quarternary times. This is amply evident from the recurrent seismic episodes, geomorphic developments, and from the geodetic changes (Valdiya, 1999). This region shows the development of all four morphotectonic zones, which are demarcated by the intracrustal boundary thrust of regional dimensions. These zones from the south to the north are Siwalik or Sub Himalaya, Lesser Himalaya, Great Himalaya, and Tethys Himalaya (Paul et al., 2003). The Lesser Himalaya comprises various thrust sheets and nappes, sandwiched between the main boundary thrust (MBT) and main central thrust (MCT) at the base of the Great Himalaya. The Great Himalaya comprises mainly Kyanite-Sillimanite bearing high-grade psammatic Gneiss and Schist intruded by the anatectic Tertiary leucogranite (Paul et al., 2003).

The Kumaon Himalaya exposes all four major litho-tectonic subdivisions of the Himalaya from the south to the north. The Outer Himalaya consisting mainly of the molassic Siwalik super group of the Neo-Pliocene age is separated in the north from the Lesser Himalaya by the main boundary fault (MBF), thus exposing the highly-folded Precambrian Paleozoic sedimentary sequence with a few knappes of older crystalline rocks that are bounded by the main central thrust (MCT) in the north. The Greater or Higher Himalaya, with the north-dipping metamorphics belonging to the central crystalline zone, is separated from the thick pile of the Tethyan Paleo-Mesozoic sequence by the Martoli fault (MF).

Under a major seismicity project funded by Department of Science and Technology, Government of India, a network of eight strong-motion stations has been installed in the highly mountainous terrain of the Kumaon Himalaya. The locations of these eight stations along with the geology of the region are shown in Figure 1. The Pithoragarh region falls in the Lesser Himalayan zone and is bounded by MCT in the north and by North Almora thrust in the south. The Lesser Himalaya consists of the sediments of the Precambrian Palaeozoic and locally Mesozoic age, metamorphosed and subdivided by the thrusts with progressively older rocks towards the north. The Pithoragarh region has the exposures of an extensive sedimentary belt including an outer Krol belt and an inner Tejam-Pithoragarh belt. It consists of a thick sequence of argillo-calcareous and arenaceous sediments constituting the Garhwal super group. The Garhwal super group is divisible into the lower argillo-calacareous Tejam group, middle predominantly-arenaceous Berinag group and the upper metamorphites of the Didihat group. The Didihat group consists of complex assemblages of Phyllite, schist, amphibolite gneiss and quartzite. The strong-motion recorders placed in Sobla, Didihat and Thal are located on the metamorphosed older crystalline hard rocks, which are highly deformed, whereas the stations in Pithoragarh and Dharchula are located on the sedimentary rocks. Didihat is situated on the Askot crystallines (which is a part of the Almora crystallines). The station in Thal is situated on the quartzites of the Berinag formation. The station in Sobla is situated near the MCT and comprises crystalline rocks. The folds of the sedimentary belt of the Pithoragarh region show

the variations of strain values and degrees of shape modifications from place to place (Bhattacharya, 1999). These structural features indicate the presence of persistently active collisional stresses in that area.

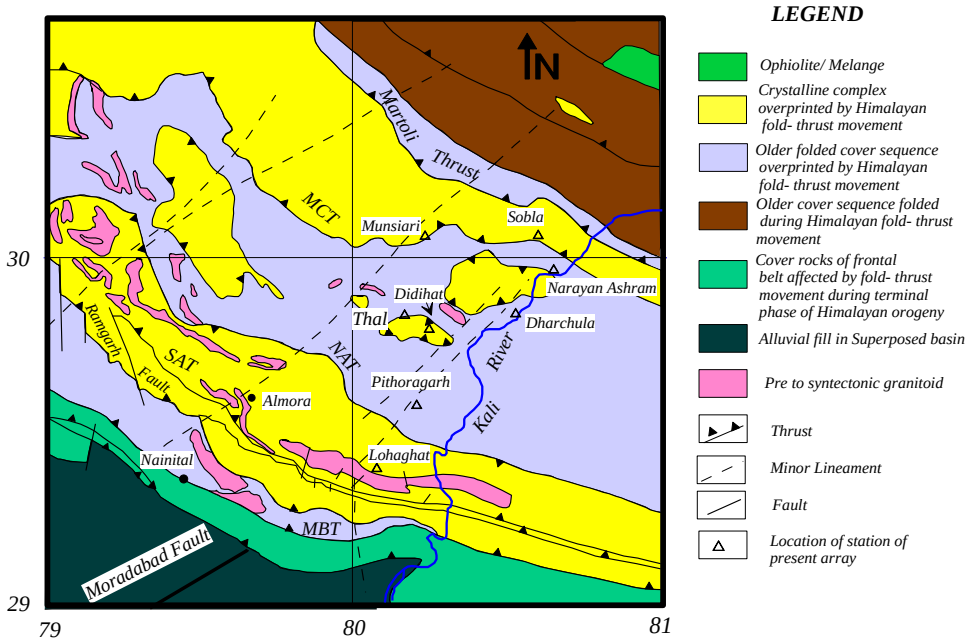

Fig. 1 Locations of the strong-motion recording stations installed in the Kumaon Himalaya (the geology and tectonics of the region are as in Dasgupta et al. (2000); the strong-motion stations of the local network are denoted by the triangles)

DATA USED IN THE ANALYSIS

The strong-motion recorders installed at each station in the network are three-component force balance accelerometers. In order to have a nearly continuous digital recording mode, the threshold level of the instruments was set at a very low level of 0.005% of the full scale. The sensitivity of the instruments is 1.25 V/g and the full-scale measurement is 2.5 V. This implies that the instruments have a very low threshold level of 0.1 Gal (0.001 m/s^2). The purpose of so low threshold level is to record almost every possible local event in the entire duration of the project. The sampling interval of digital data was kept as 0.01 s. The minimum inter-station distance between the stations of the network is approximately 11 km. Out of the eight accelerographs, seven are installed in the border district of Pithoragarh and one in the neighboring district of Champawat.

The collected accelerographs have been processed using the procedure suggested by Boore and Bommer (2005). The processing steps involve baseline correction, instrumental scaling, and frequency filtering. After the baseline and instrument corrections, a filter is generally applied to remove the high-frequency noise. In the usual processing of digital records, the California strong motion instrumentation program (CSMIP) uses the Butterworth filter with high-frequency cutoff of nearly 80% of the final sampling rate (Shakal et al., 2004). In the present work, we have the data recorded at the sampling rate of 0.01 s; therefore, on following this criterion, the high-frequency cutoff of the Butterworth filter becomes 40 Hz. The selection of the low-frequency cutoff of the Butterworth filter remains the most difficult part of strong-motion processing because the effect of increase in earthquake magnitude is to raise the response spectrum amplitudes at low frequencies. The selection of this cutoff is based on the criterion that the noise spectrum does not interfere with the usual strong-motion processing band. Hence, this depends on the characteristics of the noise and the event responsible for the record. In this work, we have selected noise from the pre-event memory of the digital records. The selection of the low cutoff of the Butterworth filter has been made in such a way that the ratio of the Fourier amplitude spectrum of the record to that of the noise is greater than 3 (Boore and Bommer, 2005). In the present work, based on the work by Boore and Bommer (2005) and Shakal et al. (2004), we have made use of the following criteria for the selection of the low-frequency cutoffs of the Butterworth filter:

- The first criterion uses the ratio of the Fourier amplitude spectrum of record to that of noise. The cutoff frequency is that frequency below which this ratio is less than 3.
- The second criterion uses the logarithms of the velocity response spectra of record and noise as originally proposed by Trifunac (1977). It is based on the observation that the logarithm of the velocity response spectrum of a record increases from low values at short periods to a maximum at intermediate periods and then starts decreasing for long periods, whereas the logarithm of the noise spectrum increases in the long-period range. The frequency, at which the ratio of the logarithms of the response spectra of record and noise is less than 3, is selected as the low-frequency corner of the Butterworth filter.
- The third criterion is based on the visual inspection of velocity and displacement time histories, which are obtained by the double integration of the acceleration record filtered by applying the Butterworth filter. The low-frequency cutoff of the Butterworth filter is based on the judgment whether or not the obtained time history shows any unusual trends.

The above criteria for the selection of the low-frequency cutoff of the Butterworth filter are shown in Figure 2. The low-frequency cutoffs of the Butterworth filter for different events recorded at different stations using these criteria are given in Table 1. One of the important steps that are used in the processing of accelerograms is padding. The padding processing step extends the time series in both directions by adding zeroes to the leading and trailing ends of the record. This step is applied before the application of the low-cut frequency filtering. The zero pads are added symmetrically to both ends of the records in order to accommodate the filter transient. The length of zero pad, t_{pad}, at each end is calculated by using the following empirically determined formula (Converse and Brady, 1992):

$$t_{\text{pad}} = \frac{1.5 \times \text{nroll}}{f_c} \tag{1}$$

where 'nroll' denotes the roll-off of the acausal low-cut Butterworth filter and f_c the low-cut frequency of the filter. The effect of padding is visible in the integrated displacement record obtained from the accelerogram. A significant value at the end of the velocity or displacement time series indicates that there may be insufficient padding. The integrated displacement record of Dharchula shows that without padding, there is a significant value at the end of the displacement record (see Figure 3(c)). The padding in the accelerogram gives a displacement record (see Figure 3(f)), which does not have significant value at the end. All records from the instruments have been processed before being used in the present work. The processed records at the Dharchula station are shown in Figure 4.

The strong-motion network installed in the Kumaon region has recorded several events from March, 2006 to February, 2007. The events, which were recorded at more than three stations, are localized by using the HYPO71 program originally developed by Lee and Lahr (1972). Table 2 gives the hypocentral parameters of these events and the obtained errors in their localization. The projections of the ray paths of the energy released from the events used in the present work to the recording stations are shown in Figure 5. It shows that at the Sobla station, the ray path of the seismic energy encounters the higher Himalayan topography, while the ray paths of the energy recorded by the other stations encounter mainly the lesser Himalayan topography.

Seismic moment is one of the most important parameters, which is required as an input to the present algorithm. This is computed from the source spectrum of the recorded data by using Brune's model (Keilis-Borok, 1959; Brune, 1970). In this process, a time window of length covering the entire S-phase is applied to the corrected accelerogram. The sampled window is cosine tapered with 10% taper at both ends (Sharma and Wason, 1994). The spectrum of this time series is obtained by using a FFT algorithm and is then corrected for the anelastic attenuation and geometrical spreading terms. For correcting anelastic attenuation, we use the frequency-dependent quality factor given by Joshi (2006), which is applicable for the Garhwal Himalaya. The plots of median source spectra of the eight events, as computed from the recorded data, are shown in Figure 6. By using the long-term flat levels in these spectra, the seismic moment of each event is calculated. Based on Brune's model (Brune, 1970), the seismic moment M_0 of an earthquake can be calculated from the long-term flat level of the displacement spectrum given by

$$M_0 = \frac{4\pi\rho\beta^3\Omega_0 R}{R_{\theta\phi}} \tag{2}$$

where ρ and β are the density and S-wave velocity of the medium, respectively, Ω_0 is the long-term flat level of the source displacement spectrum at the hypocentral distance R, and $R_{\theta\phi}$ is the radiation-pattern coefficient. We use the density of medium as 2.7 g/cm^3 (Hanks and McGuire, 1981) and shear wave velocity as 3.3 km/s (Joshi, 2000), respectively. The fault plane solution for each event used in the present work could not be determined owing to the small number of recording stations. Therefore, the radiation pattern term $R_{\theta\phi}$ for S-wave is approximately taken as 0.55 (Atkinson and Boore, 1995). In the above expression, the geometrical spreading term is taken as $1/R$. In the inversion procedure, the vertical component of a record is used to remove the possibility of site effects in the horizontal components. Therefore, in order to have consistency in the inversion procedure, source spectra are computed from the vertical components of records. For computing seismic moments from the vertical components by using the equation given above, we do not include the term, which accounts for the division of energy into two horizontal components. It is also noticed that corner frequencies for the vertical and horizontal motions will not be same. In order to keep consistency in the approach we compute source parameters from the vertical components and same components are used for inversion.

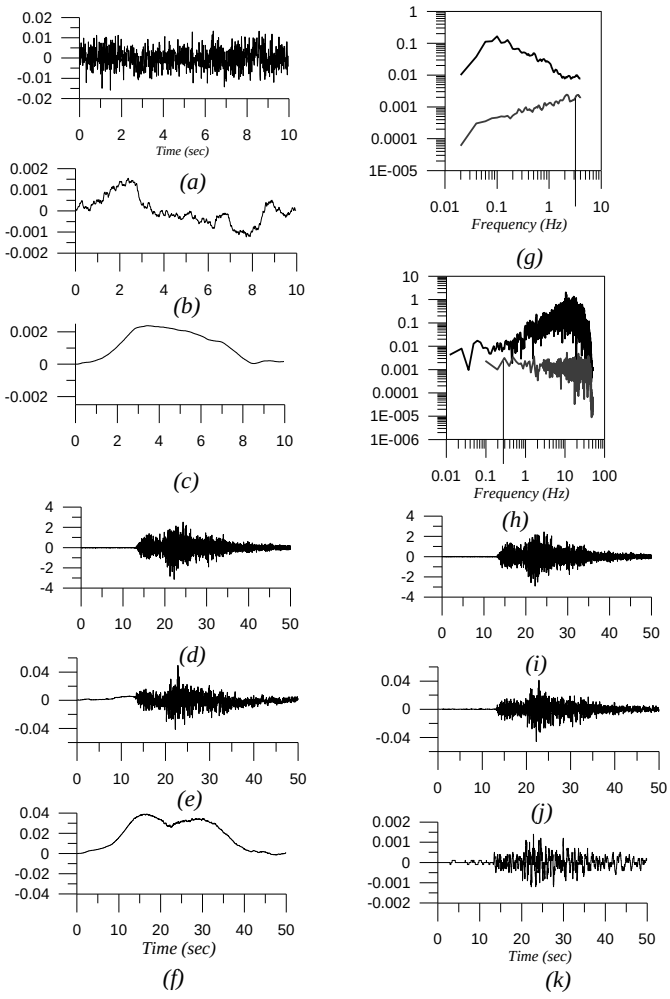

Fig. 2 (a) Acceleration, (b) velocity, and (c) displacement waveforms of the digitized record of noise taken from the pre-event memory of the record of event recorded at the Dharchula station on 05/05/06; (d) Acceleration, (e) velocity, and (f) displacement records of the signal corrupted with noise; (g) Pseudo-velocity response spectra at 5% damping of noise and signal with noise; (h) Amplitude spectra of the acceleration records of noise and signal corrupted with noise; (i) Acceleration, (j) velocity, and (k) displacement records of the signal corrupted with noise (vertical lines in the spectra denote the lower frequency cutoffs)

Table 1: Frequency Range of Low-Cut Filter Used for the Processing of Records of Strong Ground Motions of Different Events Recorded at Different Stations

Station	Date	Origin Time	F_{cl}
Pithoragarh	05/05/06	8:00:28.72	2.0
	05/08/06	7:33:00.84	2.0
	27/10/06	7:55:01.39	2.0
	05/05/06	8:49:46.48	1.8
	05/02/07	7:57:34.94	1.8
	27/10/06	8:01:32.23	1.8
Thal	05/05/06	8:00:28.72	1.5
	27/10/06	7:55:01.39	2.0
	07/05/06	6:46:03.72	1.8
	05/05/06	8:49:46.48	1.8
	05/08/06	7:33:00.84	1.9
Sobla	05/05/06	8:00:28.72	1.0
	01/04/06	19:42:52.1	1.0
	05/05/06	8:49:46.48	1.0
Didihat	05/05/06	8:00:28.72	0.7
	05/08/06	7:33:00.84	0.8
	01/04/06	19:42:52.1	0.7
	27/10/06	7:55:01.39	0.8
	05/05/06	8:49:46.48	0.8
	05/02/07	7:57:34.94	0.8
	07/05/06	6:46:03.72	0.9
Dharchula	05/05/06	8:00:28.72	1.0
	05/05/06	8:49:46.48	1.5
	01/04/06	19:42:52.1	1.5
	07/05/06	6:46:03.72	2.0
	27/10/06	7:55:01.39	1.5
	27/10/06	8:01:32.23	1.6
Note: F_{cl} denotes the lower corner of the low-cut filter used for the processing of record.			

We know that geometrical spreading term for the spherical earth model cannot be represented for all ranges by the simple power law and is not frequency-independent; however, at relatively short epicentral distances (less than a few hundred km), these effects are negligible (Yang et al., 2007). In order to check the dependency of spectral acceleration on the distance parameter we performed various numerical tests and checked the linear-, exponential- and power-law dependencies of the long-term flat level on hypocentral distance. These numerical tests are shown in Figure 7. Various statistical parameters, calculated for each dependency, are given in Table 3. It is seen that among these, the power-law dependency of the order $R^{-0.97} \sim 1/R$ gives the maximum correlation and minimum error. The mean and standard deviation from the data match effectively with those from the power-law fit. Thus, this study confirms the validity of the term $1/R$ to represent the attenuation due to geometrical spreading for the present data for both inversion and computation of the seismic moment. The geometrical factor term has been used as $1/R$ for the strong-motion studies of Himalayan and worldwide earthquakes by Boore (1983), Atkinson and Boore (1995), Joshi et al. (2001), Joshi and Midorikawa (2004) and

Joshi (2006). Since the spectral acceleration at a particular station is dependent on the geometrical spreading term, the value of this term other than $1/R$ has a direct influence on the obtained results. Therefore, the use of the geometrical term other than $1/R$ needs to be validated before using any data in a new region.

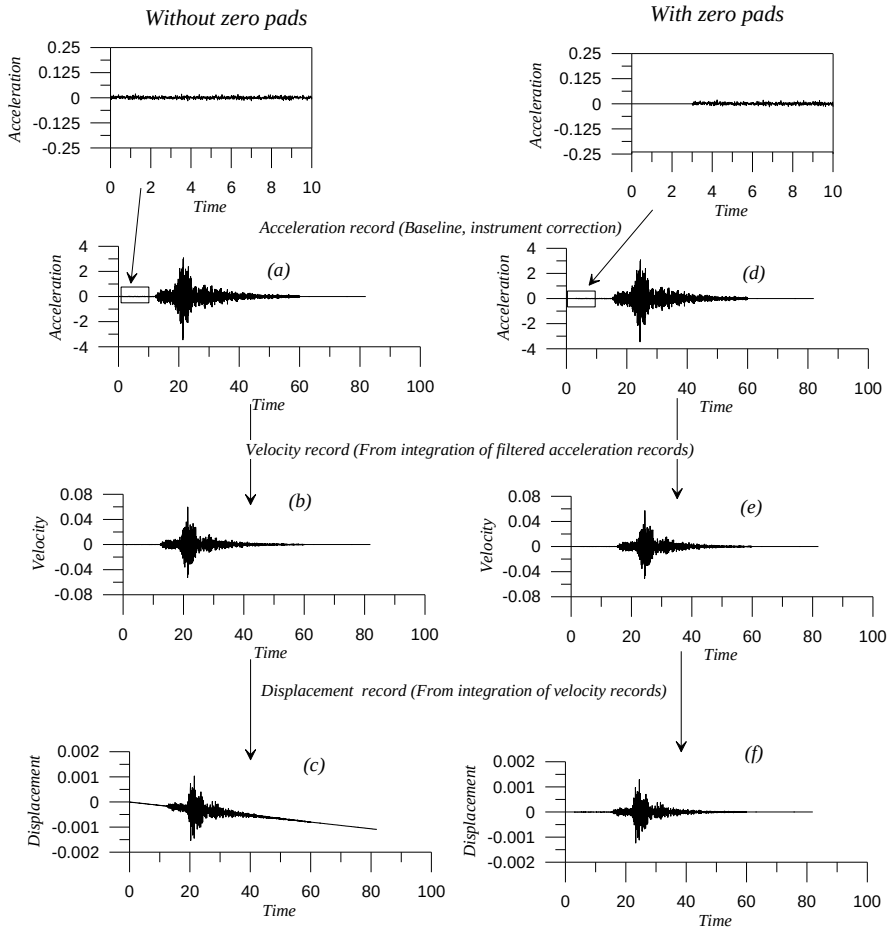

Fig. 3 (a) Acceleration record without zero pads; (b) Velocity record obtained from the integration of acceleration record; (c) Displacement record obtained from the integration of velocity record; (d) Acceleration record with zero pads; (e) Velocity record obtained from the integration of zero-padded acceleration record, and (f) Displacement record obtained from the integration of the velocity record in (e)

INVERSION

The acceleration spectrum of shear waves at distance R due to an earthquake of seismic moment M_0 can be given at frequency f as (Boore, 1983; Atkinson and Boore, 1998)

$$A(f) = CS(f, f_c)D(f) \tag{3}$$

where the term C is constant at a particular station for a given earthquake, $S(f, f_c)$ represents the source acceleration spectrum, and $D(f)$ denotes a frequency-dependent diminution function. This function modifies the spectral shape and is given as (Boore and Atkinson, 1987)

$$D(f) = \left[\frac{e^{\frac{-\pi f R}{Q(f)\beta}}}{G(R)} \right] P(f, f_{\max}) \tag{4}$$

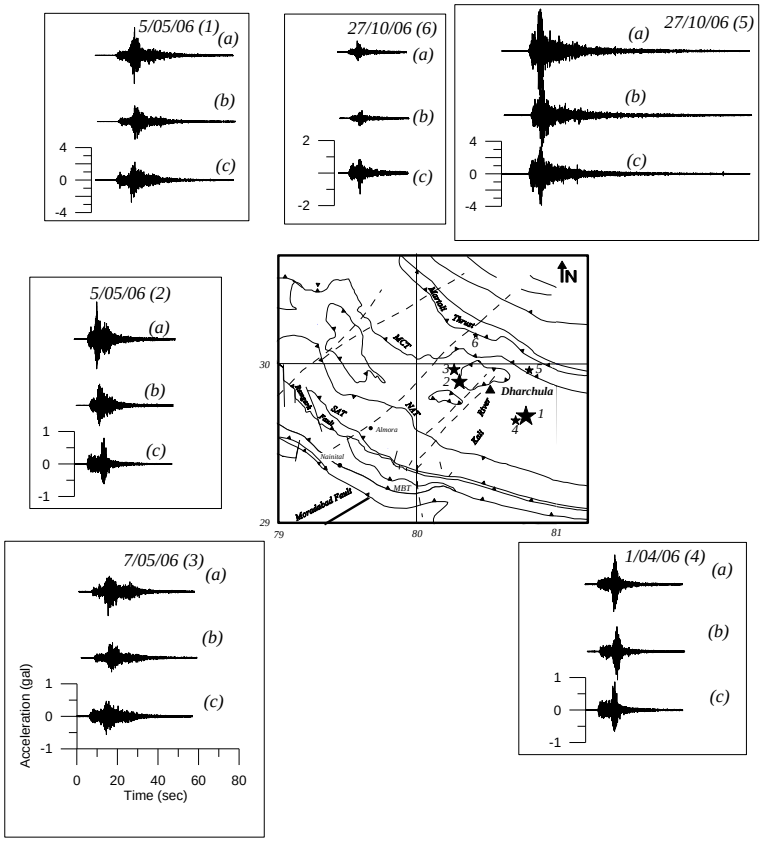

Fig. 4 Processed (a) NS, (b) EW and (c) vertical components of the accelerograms of some of the events recorded at the Dharchula station (stars denote the epicenters of events; triangles show the locations of recording stations; tectonics of the region is taken as in Dasgupta et al. (2000); number assigned to each record in brackets corresponds to the event given in Table 2)

Table 2: Estimated Hypocentral Parameters of Different Events Used in the Present Work and the Errors Obtained in Their Localization

Date	Origin Time	Epicenter	Depth (km)	M_0 ($\times 10^{22}$ dyne-cm)	Number of Stations	Error in Depth (km)
05/05/06 (1)	08:00:28.72	29º 38.65', 80º 42.16'	30	0.62	5	2.7
05/05/06 (2)	08:49:46.48	29º 40.43', 80º 45.98'	25	0.12	5	4.2
07/05/06 (3)	06:46:03.72	29º 57.57', 80º 47.89'	35	0.10	3	14.1
01/04/06 (4)	19:42:52.1	30º 10.14', 80º 24.63'	10	0.043	3	6.5
27/10/06 (5)	07:55:01.39	29º 57.46', 80º 15.23'	13	0.21	5	5.6
27/10/06 (6)	08:01:32.23	29º 52.35', 80º 17.70'	16	0.29	5	3.1
05/08/06 (7)	07:33:00.84	29º 52.61', 80º 06.88'	25	1.9	3	2.1
05/02/07 (8)	07:57:34.94	29º 52.18', 80º 16.94'	32	0.71	3	1.9
Note: The number assigned to each event is used in Figure 4.						

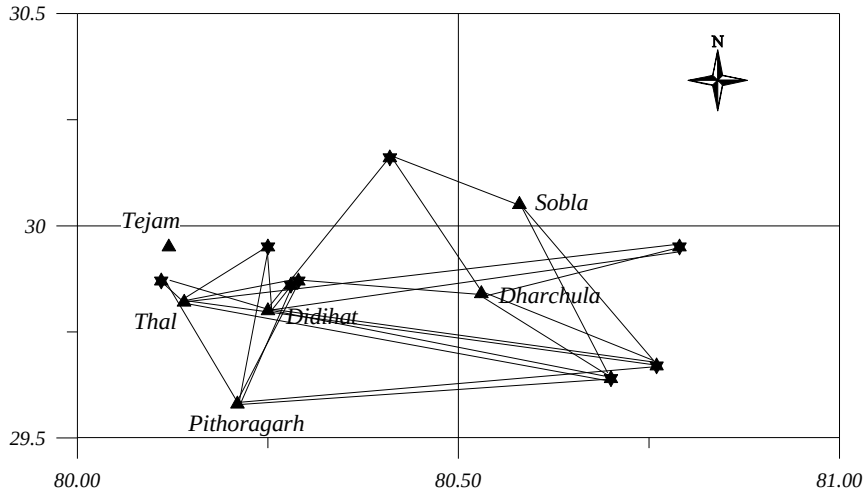

Fig. 5 Projections of the ray paths of different events recorded at different stations (stars denote the epicenters of studied earthquakes and triangles denote the locations of recording stations)

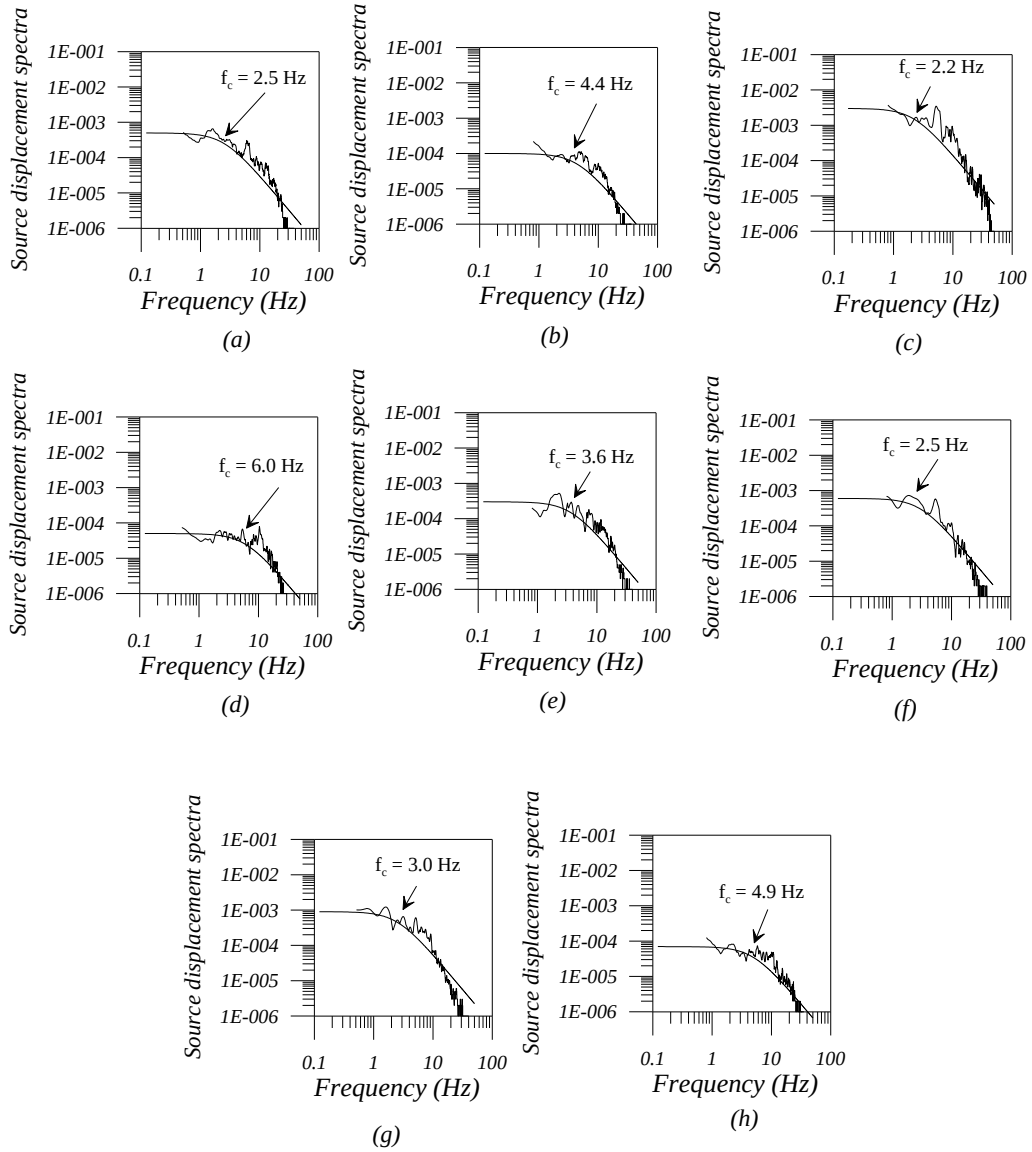

Fig. 6 Median source displacement spectra obtained for various events used for the present study (the theoretical Brune's displacement spectrum is shown in solid line)

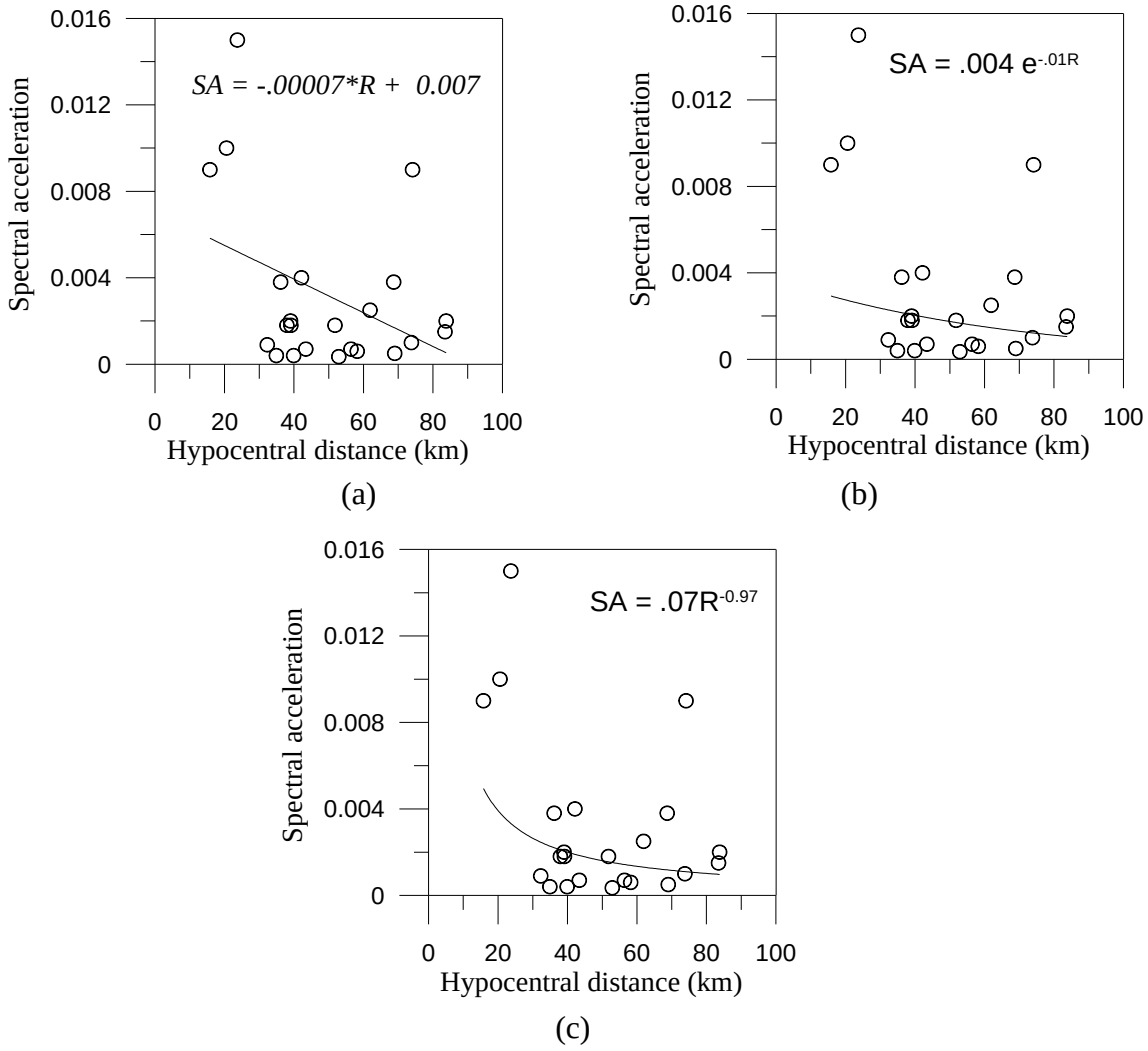

Fig. 7 (a) Linear-, (b) exponential- and (c) power-law dependence of spectral acceleration data used in the present work on hypocentral distance (the parameters SA and R are long-term flat level and hypocentral distance, respectively)

Table 3: Dependence of Spectral Acceleration on Hypocentral Distance

Type of Fit	Obtained Relation for SA	Mean (Data)	S.D. (Data)	Mean (Fit)	S.D. (Fit)	Error Sum of Square	Residual Sum of Square	Correlation Coefficient
Linear	$-0.00007R+0.007$	3.817	0.433	−4.96	0.00004	8.78	12.42	0.706
Expo-nential	$0.004e^{-0.01R}$	3.817	0.433	−5.59	0.00006	9.42	9.41	0.706
Power	$0.07R^{-0.97}$	3.817	0.433	3.52	1.054	1.01	1.09	0.733

In Equation (4), $P(f, f_{\max})$ is a high-cut filter and $e^{\frac{-\pi fR}{Q(f)\beta}} \Big/ G(R)$ is the filter used to define the anelastic attenuation and geometrical spreading of the seismic energy. As we are using the data from those events, which lie at the hypocentral distances ≤ 100 km, $G(R)$ is assumed as $1/R$ (Singh et al., 2006). The term $Q_\beta(f)$ used in Equation (4) is the frequency-dependent shear wave quality factor. In this work we take f_m as 50 Hz, which is the Nyquist frequency of the processed records at a sampling

interval of 0.01 s. This expression serves as the basis for our inversion. For a double-couple seismic source embedded in an elastic medium, on considering only S-waves, C is given as (Boore, 1983)

$$C = \frac{M_0 R_{\theta\phi} \mathrm{FS}}{4\pi\rho\beta^3} \tag{5}$$

In this expression M_0 is the seismic moment, $R_{\theta\phi}$ is the radiation pattern, FS is the amplification due to free surface, and ρ and β are the density of the medium and the shear wave velocity, respectively. In the present work we have used the values of the parameters $R_{\theta\phi}$ and FS as 0.55 and 2.0, respectively (Atkinson and Boore, 1995). The density of the medium and the shear wave velocity in Himalaya have been assumed as 2.7 g/cm^3 (Hanks and McGuire, 1981) and 3.3 km/s (Joshi, 2000), respectively. The filter $S(f, f_c)$ in Equation (3) defines the source spectrum of the earthquake. On using the spectral shape based on the ω^{-2} decay of high frequency proposed by Aki and Chouet (1975) and Brune (1970), $S(f, f_c)$ is defined as

$$S(f, f_c) = \frac{(2\pi f)^2}{1 + \left(\frac{f}{f_c}\right)^2} \tag{6}$$

Further, Equation (3) is linearized by taking its natural logarithm to become

$$\ln A(f) = \ln C + \ln S(f, f_c) - \frac{\pi f R}{Q_\beta(f)\beta} - \ln R + \ln P(f, f_{\max}) \tag{7}$$

where $Q_\beta(f)$ and f_c are unknown. The term representing the source filter $S(f, f_c)$ can be replaced with the help of Equation (3). Further, with the assumption that f_c is known, we are left with only one unknown, $Q_\beta(f)$. On rearranging the known and unknown quantities on different sides, we obtain the following form from Equation (7):

$$\frac{-\pi f R}{Q_\beta(f)\beta} = \ln A(f) - \ln C - \ln S(f, f_c) + \ln R - \ln P(f, f_{\max}) \tag{8}$$

We obtained following set of equations at the 1st recording station for the *i*th earthquake for the frequencies f_1, f_2, f_3 ..... f_n, where n denotes the total number of digitized samples in the acceleration record:

$$\frac{-\pi f_1 R_{i1}}{Q_\beta(f_1)\beta} + e = D_{i1}(f_1) \tag{9}$$

$$\frac{-\pi f_2 R_{i1}}{Q_\beta(f_2)\beta} + e = D_{i1}(f_2) \tag{10}$$

$$\vdots \qquad \vdots \qquad \vdots$$

$$\frac{-\pi f_n R_{i1}}{Q_\beta(f_n)\beta} + e = D_{i1}(f_n) \tag{11}$$

In these expressions, $D_{i1}(f_k)$ is given as (for j = 1)

$$D_{ij}(f_k) = \ln A(f_k) - \ln C - \ln\left(S(f_k, f_c)\right) + \ln R_{ij} - \ln P(f_k, f_{\max}); \quad k = 1, 2, 3, \ldots, n \tag{12}$$

where the subscripts i and j in the parameters $D_{ij}(f_k)$ and R_{ij} represent the event and station number, respectively. In the matrix form, the above set of equations at the 1st recording station for m number of earthquakes can be written as

$$
\begin{vmatrix}
\frac{-\pi f_1 R_{11}}{\beta} & 0 & 0 & \ldots\ldots\ldots\ldots & 0 & 1 \\
0 & \frac{-\pi f_2 R_{11}}{\beta} & 0 & \ldots\ldots\ldots\ldots & 0 & 1 \\
0 & 0 & \frac{-\pi f_3 R_{11}}{\beta} & \ldots\ldots\ldots\ldots & 0 & 1 \\
\vdots & \vdots & \vdots & & \vdots & \vdots \\
0 & 0 & 0 & \ldots\ldots\ldots & \frac{-\pi f_n R_{11}}{\beta} & 1 \\
 & & & \vdots & & \\
 & & & \text{for } m\text{th earthquake} & & \\
\frac{-\pi f_1 R_{m1}}{\beta} & 0 & 0 & \ldots\ldots\ldots\ldots & 0 & 1 \\
0 & \frac{-\pi f_2 R_{m1}}{\beta} & 0 & \ldots\ldots\ldots\ldots & 0 & 1 \\
0 & 0 & \frac{-\pi f_3 R_{m1}}{\beta} & \ldots\ldots\ldots\ldots & 0 & 1 \\
\vdots & \vdots & \vdots & & \vdots & \vdots \\
0 & 0 & 0 & \ldots\ldots\ldots & \frac{-\pi f_n R_{m1}}{\beta} & 1
\end{vmatrix}
\begin{vmatrix}
\frac{1}{Q_\beta(f_1)} \\
\frac{1}{Q_\beta(f_2)} \\
\frac{1}{Q_\beta(f_3)} \\
\vdots \\
\frac{1}{Q_\beta(f_n)} \\
e
\end{vmatrix}
=
\begin{vmatrix}
D_{11}(f_1) \\
D_{11}(f_2) \\
D_{11}(f_3) \\
\vdots \\
D_{11}(f_n) \\
\vdots \\
D_{m1}(f_1) \\
D_{m1}(f_2) \\
D_{m1}(f_3) \\
\vdots \\
D_{m1}(f_n)
\end{vmatrix}
\tag{13}
$$

This can be represented in the following form:

$$[G]\{m\} = \{d\} \tag{14}$$

The rectangular matrix $[G]$ in Equation (14) represents the first rectangular matrix in Equation (13), the column matrix $\{m\}$ represents the column matrix on the left hand side of Equation (13) and the column matrix $\{d\}$ represents the column matrix on the right hand side of Equation (13). In Equation (14), the model parameters are contained in the model matrix $\{m\}$ and the spectral components in the data matrix $\{d\}$. Inversion of the $[G]$ matrix gives the estimated model matrix $\{m\}$ on using the Newton's method as

$$\{m\}_{\text{est}} = \left([G]^T [G]\right)^{-1} [G]^T \{d\} \tag{15}$$

The above inversion is prone to problems if $[G]^T [G]$ is even close to being singular and for such cases, we can solve for $\{m\}$ by using the singular value decomposition (SVD) (Press et al., 1992). Formulation for the SVD-based solution follows Lanczos (1961). In this formulation, the $[G]$ matrix is decomposed into $[V_p]$, $[U_p]$ and $[\Lambda_p]$ matrices as given by Fletcher (1995):

$$[G]^{-1} = [V_p][\Lambda_p][U_p]^T \tag{16}$$

where $\left[V_p\right]$, $\left[U_p\right]$ and $\left[\Lambda_p\right]$ are the matrices having non-zero singular vectors and singular values. For the present work, the software QINV developed by Joshi (2006) has been modified and used. We have computed root-mean-square error (RMSE) between the elements of input data matrix and estimated data matrix in each iteration and this is used as the basis for the selection of final model. In the present inversion, we have performed a grid search for f^c.We use the initial values of f^c as 0.01 Hz and then it is increased in Δf_c increments of 0.01 Hz up to 10.0 Hz. A tree diagram for the selection of corner frequencies of different events is shown in Figure 8. We get different solutions for different possibilities of f^c. The final solution is that which gives the minimum RMSE.

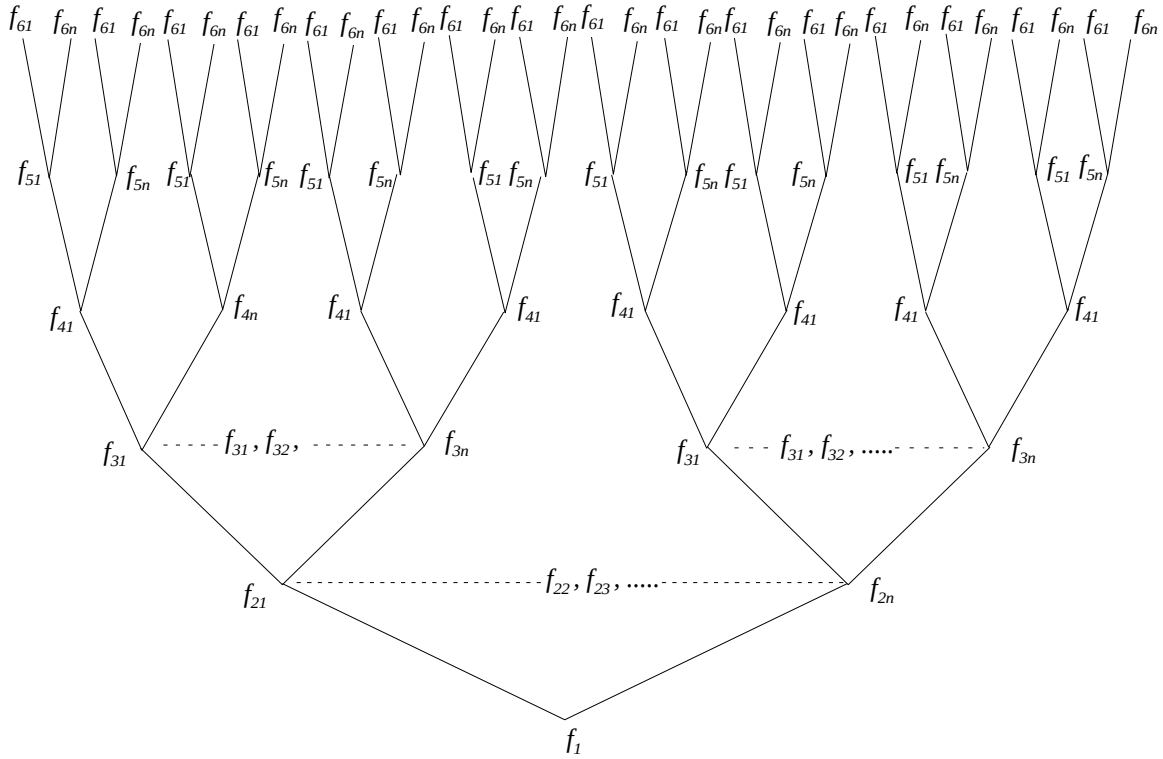

Fig. 8 Tree for the search of corner frequencies of various events (the tree diagram is shown for only two nodes; however, there will be several nodes between f_{21} to f_{2n}, f_{31} to f_{3n}, etc., where f_{21} denotes the corner frequency of second event with first value and f_{2n} denotes the corner frequency of second event with last value; the present tree diagram is for one value of f_1; however, in the present algorithm this also varies from 1 to n; for simplicity in the diagram n is kept same for all events; however, in actual algorithm n can be different for different events)

Due to the presence of site amplification effects in the horizontal component of the records we have used the vertical component of a record as an input to the algorithm. The spectrum of S-phase in the corrected accelerogram has been used as an input to the inversion algorithm developed in this paper. A time window, which starts from the onset of S-phase in the record and covers the entire S-phase, has been applied to the corrected accelerogram. This sampled window is cosine tapered with 10% taper at both ends (Sharma and Wason, 1994). The so-obtained spectrum is further smoothened before being used as an input to the present algorithm. The complete process of obtaining spectral amplitudes from the processed time series is shown in Figure 9. The whole algorithm is designed in such a manner that the input of acceleration spectra of different events is given in an order of increasing seismic moment. The value of so-obtained $Q_\beta(f)$ corresponds to different frequencies at different stations.

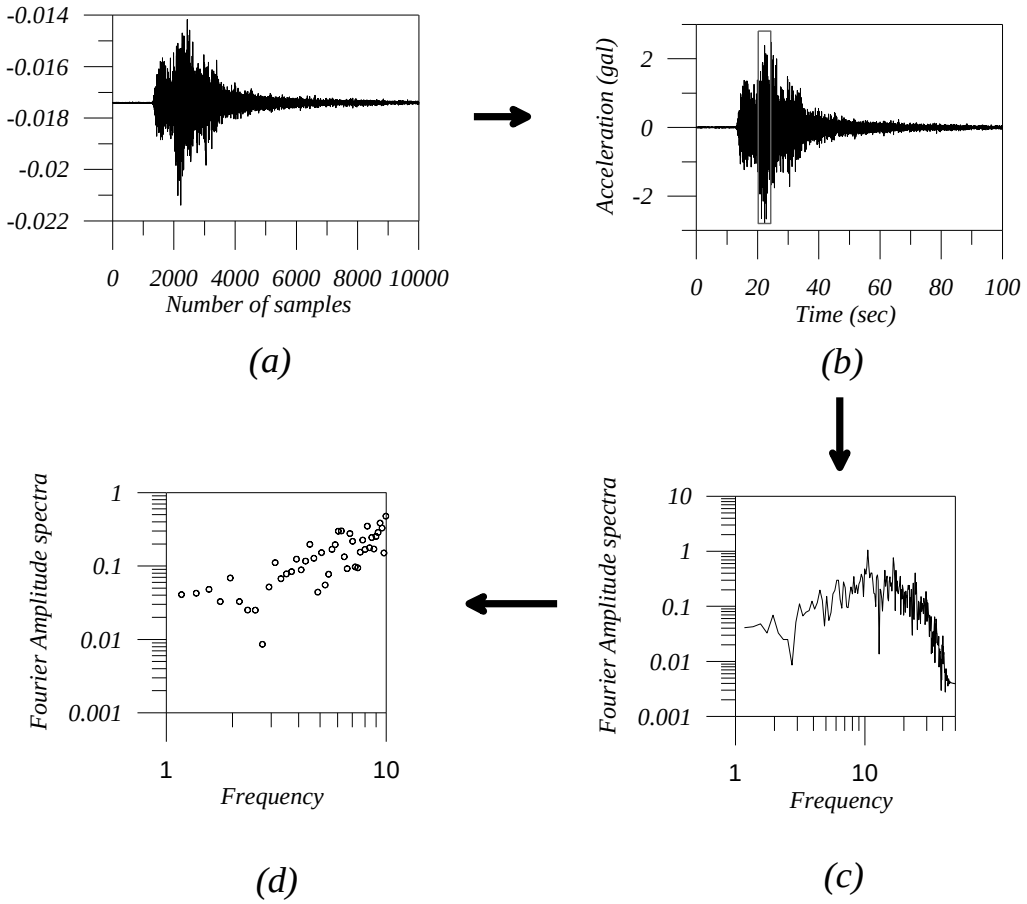

Fig. 9 (a) Vertical component of unprocessed accelerogram of 05/05/06 event recorded at Dharchula station; (b) Processed accelerogram at Didihat station; (c) Acceleration spectrum of S-phase marked by rectangular block with a time window of 4.0 s; (d) Discrete value of acceleration spectra used for present inversion (the discrete values of acceleration spectra are shown by small circles)

RESULTS AND DISCUSSION

A numerical experiment is performed in which the time window has been changed and its relation with RMSE is observed for deriving the $Q_\beta(f)$ relationship for the station at Pithoragarh. We have taken records from six events recorded at this station, which are given in Table 1. It is seen that the selection of window in this approach is dependent on the S-phase present in the record. The S-phase is small for the near-field events while it is large for the far-field or distant earthquakes. The minimum time window for the S-phase is 3 s in the case of data recorded at Pithoragarh station for the event recorded on 5/08/06. We have changed the time window to 2.5, 3.0, 3.5, 4.0 and 7.0 s. The error obtained and its dependence on time window is shown in Figure 10. The so-obtained relation and errors for different time windows are given in Table 4. It is seen that the minimum error is obtained for the case of 3.0-s time window and that it increases when this window is either increased or decreased. This may be due to the overlapping of other phases in the input record for larger time windows and incomplete S-phases in smaller time windows. This experiment shows that a proper choice of window has strong influence on the obtained $Q_\beta(f)$ structure. On repeating this experiment on other stations, it has been seen that the selection of time window is decided by the shortest time window which covers the complete S-phase in the near-field record at any station. Further, in a separate numerical experiment a comparatively high RMSE was observed when we used different windows for different records as input to the algorithm.

Table 4: Dependence of Obtained $Q_\beta(f)$ Relationship on Time Window

Length of Time Window (s)	Obtained Relation	RMSE
2.5	$Q_\beta(f) = 186 f^{0.72}$	0.000028
3.0	$Q_\beta(f) = 73 f^{1.28}$	0.000011
3.5	$Q_\beta(f) = 181 f^{0.64}$	0.000056
4.0	$Q_\beta(f) = 36 f^{1.56}$	0.00017
7.0	$Q_\beta(f) = 15 f^{1.24}$	0.00143

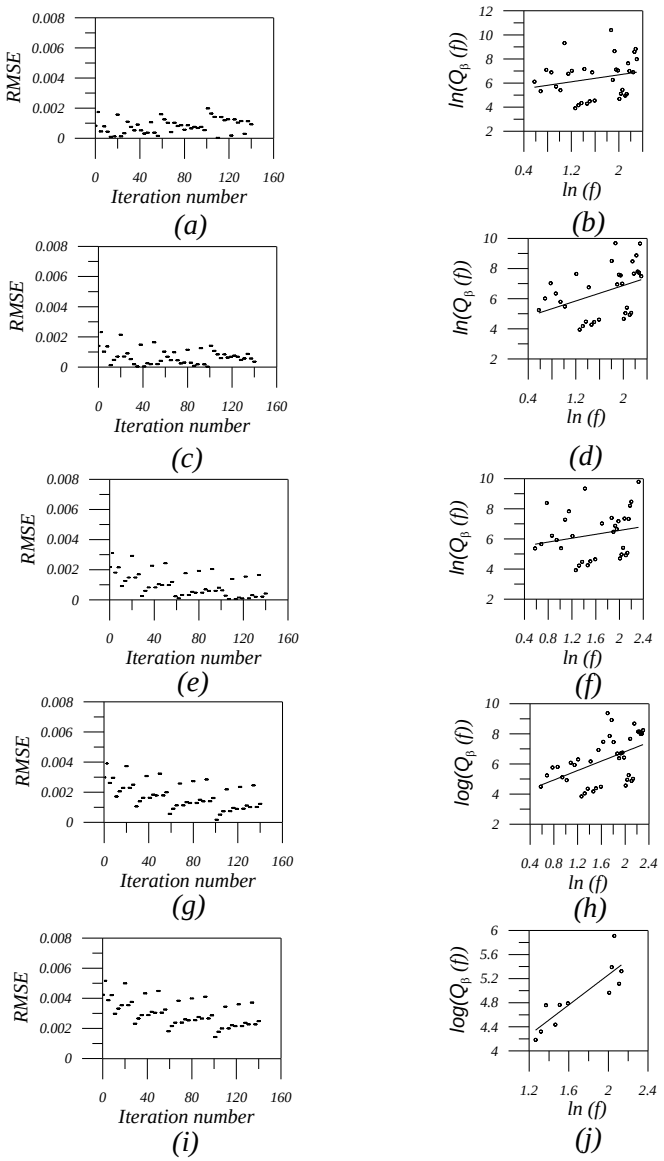

Fig. 10 Dependence of time window on the obtained results (the error plots for time windows of 2.5, 3.0, 3.5, 4.0 and 7.0 s are shown in (a), (c), (e), (g) and (i), respectively; the obtained $Q_\beta(f)$ relationships for the spectra of input time windows of 2.5, 3.0, 3.5, 4.0 and 7.0 s are shown in (b), (d), (f), (h) and (j), respectively)

This inversion algorithm is also dependent on the selection of corner frequency for individual events. We have devised a tree in which the corner frequency of input events is changed in an iterative manner.

Some of the results of this iterative inversion for the data at Pithoragarh stations for the input time window of 2.5 s are shown in Figure 11. The error plot corresponding to the different values of selected corner frequencies and their dependence on RMSE is shown in Figure 11(a). The corresponding relation and the set of corner frequencies for the so-obtained $Q_\beta(f)$ are shown in Table 5.

Table 5: Different Sets of Corner Frequencies and the Corresponding Errors in the Observed Relation

S. No.	Corner Frequency of Input Events	RMSE
Case 1	f_{c1} = 1.9, f_{c2} = 2.0, f_{c3} = 2.0, f_{c4} = 2.4, f_{c5} = 2.4, f_{c6} = 6.4	.0019
Case 2	f_{c1} = 1.9, f_{c2} = 2.0, f_{c3} = 2.0, f_{c4} = 2.4, f_{c5} = 3.2, f_{c6} = 6.4	.0016
Case 3	f_{c1} = 1.9, f_{c2} = 2.0, f_{c3} = 2.0, f_{c4} = 2.4, f_{c5} = 4.0, f_{c6} = 6.4	.0014
Case 4	f_{c1} = 1.9, f_{c2} = 2.0, f_{c3} = 2.0, f_{c4} = 3.6, f_{c5} = 4.0, f_{c6} = 6.4	.000028
Case 5	f_{c1} = 1.9, f_{c2} = 2.0, f_{c3} = 3.0, f_{c4} = 3.6, f_{c5} = 4.0, f_{c6} = 6.4	.0014
Case 6	f_{c1} = 1.9, f_{c2} = 2.0, f_{c3} = 2.0, f_{c4} = 2.4, f_{c5} = 4.8, f_{c6} = 6.4	.0012
Case 7	f_{c1} = 1.9, f_{c2} = 2.0, f_{c3} = 2.0, f_{c4} = 3.6, f_{c5} = 4.8, f_{c6} = 6.4	.0012

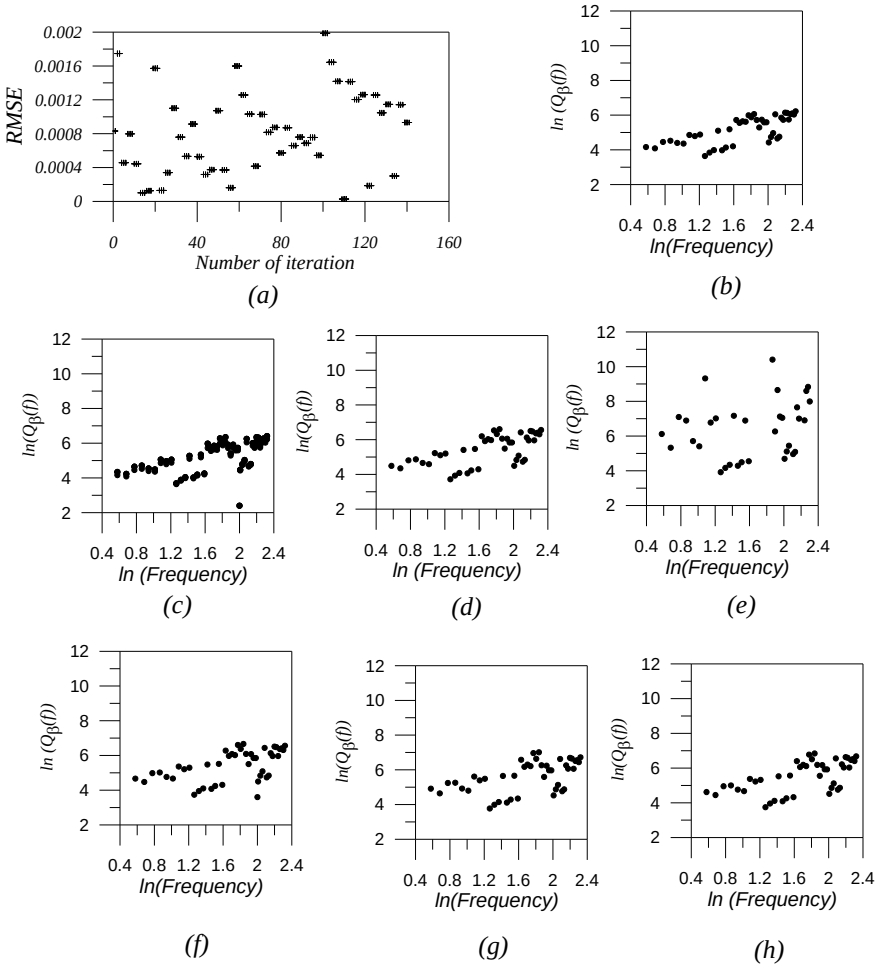

Fig. 11 (a) RMSEs for different iterations corresponding to different values of corner frequencies of selected events; Plots of $Q_\beta(f)$ versus frequency for (b) Case 1, (c) Case 2, (d) Case 3, (e) Case 4, (f) Case 5, (g) Case 6 and (h) Case 7 (the corner frequencies corresponding to different cases are given in Table 4)

Before arriving at the final $Q_\beta(f)$ relationship at each station, various time windows were considered and their effect on RMSE was observed at different stations. Table 6 shows the $Q_\beta(f)$ relation that corresponds to the minimum RMSE for the selected time window at different stations. A plot of the so-obtained variation of $Q_\beta(f)$ with frequency at different stations is shown in Figure 12. It is seen that high Q_0 is obtained at the Didihat and Sobla stations while a low value of Q_0 is obtained at the Dharchula station. RMSE is low at Pithoragarh, Dharchula and Didihat stations at which we have used the input of six and seven events, respectively. Maximum RMSE is obtained at the Sobla station where we have used the data of only three events. High RMSE is also observed at the Thal station where we have used the data of only five events. As the whole area covers the Pithoragarh region, which is mostly covered by the sequences of Lesser Himalaya, we have plotted the $Q_\beta(f)$ values obtained from inversion at all stations to obtain a regional relationship. In order to maintain the reliability of this relationship we have selected data in the frequency band of 2.0–10.0 Hz, which covers the maximum low-frequency cutoff and minimum high-frequency cutoff of the band-pass filter used in the processing of various records. The plot of $Q_\beta(f)$ versus frequency is shown in Figure 13 and the best-fit line gives a regional frequency-dependent relation as $30 f^{1.45}$ which is applicable to the Pithoragarh region.

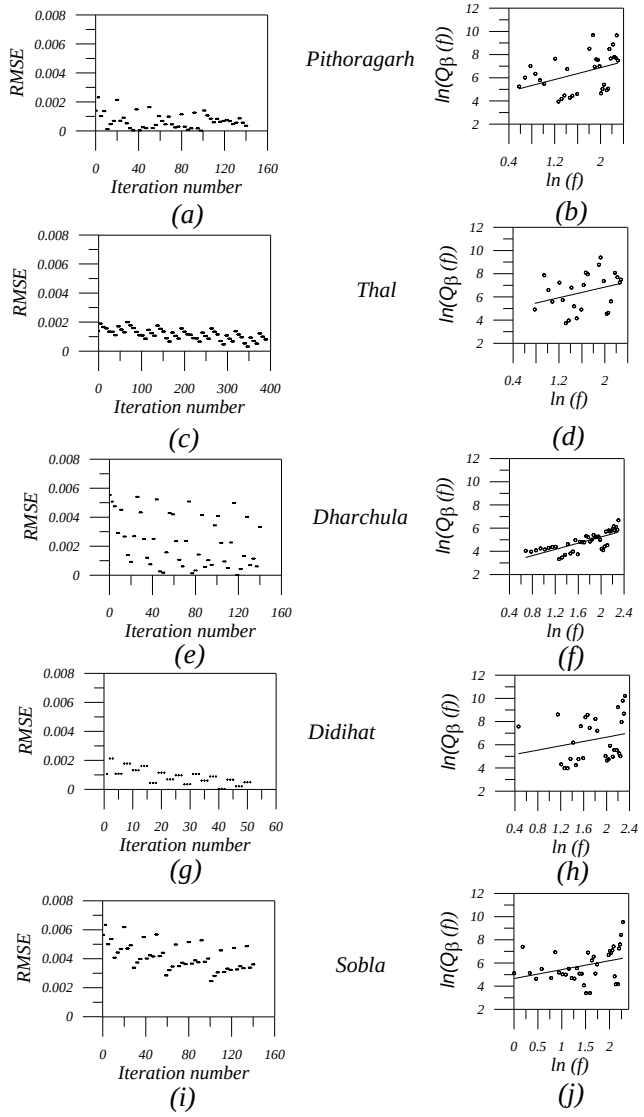

Fig. 12 Plots of RMSE at (a) Pithoragarh, (c) Thal, (e) Dharchula, (g) Didihat and (i) Sobla stations for various iterations; Plots of $Q_\beta(f)$ at (b) Pithoragarh, (d) Thal, (f) Dharchula, (h) Didihat and (j) Sobla

Table 6: $Q_\beta(f)$ Relations Obtained at Various Stations

Station	Relation	RMSE
Pithoragarh	$73f^{1.28}$	.000011
Thal	$94f^{1.14}$	.000318
Dharchula	$13f^{1.3}$	.000015
Didihat	$120f^{0.93}$	.000036
Sobla	$105f^{0.76}$	.001442

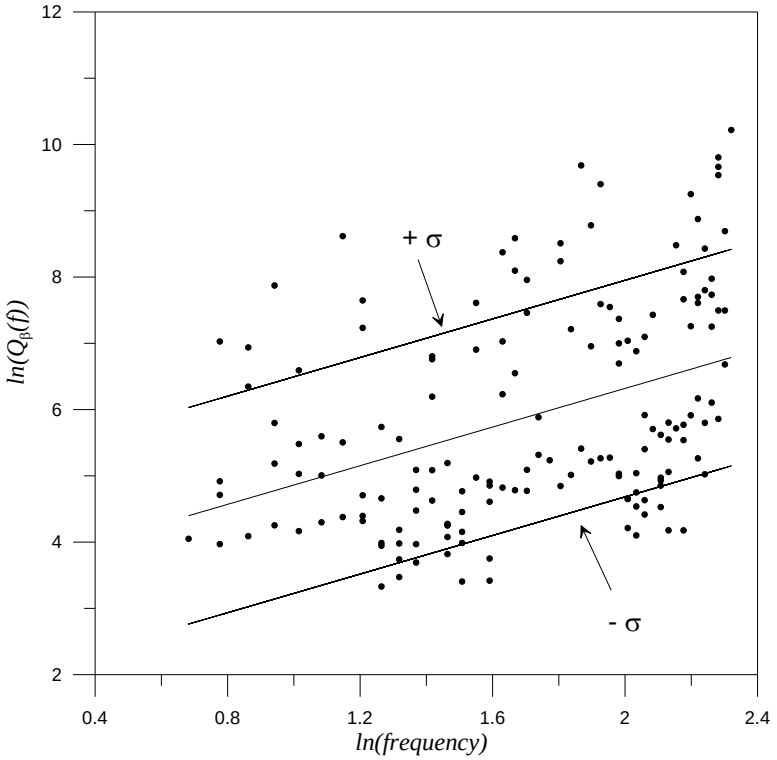

Fig. 13 Average $Q_\beta(f)$ relationship for Pithoragarh region based on the obtained values of shear wave attenuation at different stations at different frequencies

It is seen that although Q is probably constant over a large frequency range in homogeneous material, this is not the case in inhomogeneous media (van der Baan, 2002). At regional distances, estimates typically show an approximately constant Q for frequencies 0.28×10^{-4} to 0.1 Hz (i.e., periods 10 s to 1 hr) and increase with frequency for frequencies greater than 1.0 Hz (Dziewonski, 1979; Sipkin and Jordan, 1979; Sato and Fehler, 1997). For S-waves at frequencies 1 to 25 Hz, Q is proportional to f^n with n ranging between 0.6 and 0.8 on average (Aki, 1980; Sato and Fehler, 1997). The frequency-dependent Q relation can be used to characterize the tectonic nature of the region. The relation $Q(f) = Q_0 f^n$ generally provides Q_0 which represents heterogeneities and n represents the level of tectonic activity of the region. Regions with higher n values manifest higher tectonic activity. Various studies defining the relations of frequency-dependent quality factors show that for various active regions like Guerrero (Mexico), Yugoslavia, Hindukush, South Iberia, South Spain, Garhwal Himalaya (India), North-East Himalaya (India), North-West Himalaya (India), Koyna (India), etc., Q_0 and n vary from 47 to 169 and 0.7 to 1.05, respectively (Rodriguez et al., 1983; Rovelii, 1984; Roecker et al., 1982; Pujades et al., 1990; Ibanez et al., 1990; Gupta et al., 1995; Paul et al. 2003; Gupta and Kumar, 2002; Kumar et al., 2005; Mandal and Rastogi, 1998; Gupta et al., 1998). For the stable regions like Norway, South Carolina

and North Iberia the values of Q_0 and n vary from 190 to 600 and from 0.45 to 1.09, respectively (Kvamme and Havskov, 1989; Rhea, 1984; Pujades et al., 1990). A low Q_0 (< 200) and high n (> 0.8) value in the relation of frequency-dependent quality factor suggests that the region is tectonically and seismically active (Kumar et al., 2005). A low Q_0 and high n value in the developed relation for Kumaon Himalaya suggests a high level of tectonic activity in this part of the region.

Corner frequency is one of the main parameters, which is obtained from source spectra. In the present algorithm, seismic moment is used as one of the inputs. Although long-term flat level from source spectra is used for calculating seismic moment, the role of corner frequency in designing the source spectra cannot be ruled out. The corner frequency obtained from the source spectra of each event at different stations is compared with that obtained from inversion in Figure 14. It is seen that the obtained values of corner frequency of event at different stations from these two approaches do not differ significantly. However, in order to have complete unbiasness of results we need to include seismic moment in inversion at the cost of increased unknown parameters.

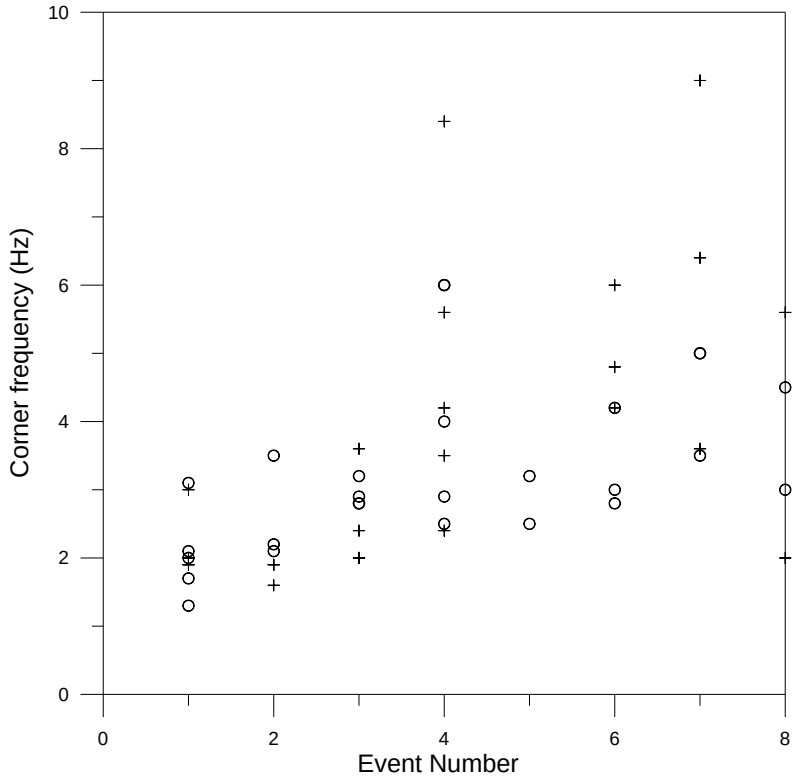

Fig. 14 Comparison of corner frequencies obtained at different stations from source displacement spectra and from present inversion (the crosses and circles show the values of corner frequencies obtained from source displacement spectra and present inversion, respectively; the *x*-axis shows the numbers corresponding to various events)

It may be mentioned that a $Q_\beta(f)$ relationship is directly used in various techniques of simulation of strong ground motion like semi-empirical modeling technique (Joshi et al., 2001; Joshi and Midorikawa, 2004), composite source-modelling technique (Zeng et al., 1994), and stochastic simulation technique (Boore, 1983). Therefore, an estimate of $Q_\beta(f)$ not only serves purpose for the attenuation properties of the region but it is also among the useful parameters needed for a successful prediction of strong ground motion for engineering use in any region as it controls shear wave attenuation in the region.

CONCLUSIONS

In this paper, an effective algorithm for obtaining $Q_\beta(f)$ relations from strong-motion data has been presented. The data of eight events recorded at five stations located in the Pithoragarh region of Kumaon Himalayas from a local strong-motion network has been used in this study. The final $Q_\beta(f)$ is based on the solution, which gives minimum root-mean-square error in the inversion algorithm. Using recorded strong motions different $Q_\beta(f)$ relations are obtained at different stations. The $Q_\beta(f)$ obtained at different stations from inversion is used to obtain a regression relation of $Q_\beta(f) = 30\, f^{1.45}$, which is applicable in a frequency range of 2.0–10.0 Hz. This $Q_\beta(f)$ relation shows that the Pithoragarh region is seismically active and is characterized by local heterogeneities. Besides estimating the nature of material between the source of an earthquake and the observation point, the developed $Q_\beta(f)$ relation can be used for a realistic simulation of strong ground motions by using the stochastic simulation technique in this part of Himalayas.

ACKNOWLEDGEMENTS

The authors sincerely thank Department of Science and Technology, India, Indian Institute of Technology, Roorkee, Kurukshetra University, and National Geophysical Research Institute for supporting the research presented in this paper. The work presented in this paper is an outcome of the DST project grant No. DST/23(483)/SU/2004, Government of India.

REFERENCES

1. Aki, K. and Chouet, B. (1975). “Origin of Coda Waves: Source, Attenuation and Scattering Effects”, Journal of Geophysical Research, Vol. 80, No. 23, pp. 3322–3342.
2. Aki, K. (1980). “Attenuation of Shear Waves in the Lithosphere for Frequencies from .05 to 25 Hz”, Physics of the Earth and Planetary Interiors, Vol. 21, No. 1, pp. 50–60.
3. Atkinson, G.M. and Boore, D.M. (1995). “Ground Motion Relations for Eastern North America”, Bulletin of the Seismological Society of America, Vol. 85, No. 1, pp. 17–30.
4. Atkinson, G.M. and Boore, D.M. (1998). “Evaluation of Models for Earthquake Source Spectra in Eastern North America”, Bulletin of the Seismological Society of America, Vol. 88, No. 4, pp. 917–934.
5. Bhattacharya, A.R. (1999). “Deformational Regimes across the Kumaun Himalayas: A Study in Strain Patterns” in “Geodynamics of the NW Himalaya (edited by A.K. Jain and R.M. Manickvasgam)”, Gondwana Research Group Memoir No. 6, Field Science, Osaka, Japan.
6. Boore, D.M. (1983). “Stochastic Simulation of High-Frequency Ground Motions Based on Seismological Models of the Radiated Spectra”, Bulletin of the Seismological Society of America, Vol. 73, No. 6A, pp.1865–1894.
7. Boore, D.M. and Atkinson, G.M. (1987). “Stochastic Prediction of Ground Motion and Spectral Response Parameters at Hard-Rock Sites in Eastern North America”, Bulletin of the Seismological Society of America, Vol. 77, No. 2, pp. 440–467.
8. Boore, D.M. and Bommer, J. (2005). “Processing of Strong Motion Accelerograms: Needs, Options and Consequences”, Soil Dynamics and Earthquake Engineering, Vol. 25, No. 2, pp. 93–115.
9. Brune, J.M. (1970). “Tectonic Stress and the Spectra of Seismic Shear Waves from Earthquakes”, Journal of Geophysical Research, Vol. 75, No. 26, pp. 4997–5009.
10. Converse, A.M. and Brady, A.G. (1992). “BAP: Basic Strong Motion Accelerogram Processing Software, Version 1.0”, Open File Report 92-296A, United States Geological Survey, Denver, U.S.A.
11. Dasgupta, S., Pande, P., Ganguly, D., Iqbal, Z., Sanyal, K., Venkatraman, N.V., Dasgupta, S., Sural, B., Harendranath, L., Mazumdar, K., Sanyal, S., Roy, A., Das, L.K., Misra, P.S. and Gupta, H. (2000). “Seismotectonic Atlas of India and Its Environs”, Geological Survey of India, Kolkata.

12. Dziewonski, A.M. (1979). "Elastic and Anelastic Structure of the Earth", Reviews of Geophysics, Vol. 17, No. 2, pp. 303–312.
13. Fletcher, J.B. (1995). "Source Parameters and Crustal Q for Four Earthquakes in South Carolina", Seismological Research Letters, Vol. 66, No. 4, pp. 44–61.
14. Gupta, S.C. and Kumar, A. (2002). "Seismic Wave Attenuation Characteristics of Three Indian Regions: A Comparative Study", Current Science, Vol. 82, No. 4, pp. 407–412.
15. Gupta, S.C., Singh, V.N. and Kumar, A. (1995). "Attenuation of Coda Waves in the Garhwal Himalaya, India", Physics of the Earth and Planetary Interiors, Vol. 87, No. 3-4, pp. 247–253.
16. Gupta, S.C., Teotia, S.S., Rai, S.S. and Gautam, N. (1998). "Coda Q Estimates in the Koyna Region, India", Pure and Applied Geophysics, Vol. 153, No.2-4, pp. 713–731.
17. Hanks, T.C. and McGuire, R.K. (1981). "The Character of High Frequency Strong Ground Motion", Bulletin of the Seismological Society of America, Vol. 71, No. 6, pp. 2071–2095.
18. Ibáñez, J.M., Del Pezzo, E., De Miguel, F., Herraiz, M., Alguacil, G. and Morales, J. (1990). "Depth-Dependent Seismic Attenuation in the Granada Zone (Southern Spain)", Bulletin of the Seismological Society of America., Vol. 80, No. 5, pp. 1232–1244.
19. Joshi, A. (2000). "Modelling of Rupture Planes for Peak Ground Accelerations and Its Application to the Isoseismal Map of MMI Scale in Indian Region", Journal of Seismology, Vol. 4, No. 2, pp. 143–160.
20. Joshi, A. (2006). "Use of Acceleration Spectra for Determining the Frequency-Dependent Attenuation Coefficient and Source Parameters", Bulletin of the Seismological Society of America, Vol. 96, No. 6, pp. 2165–2180.
21. Joshi, A. and Midorikawa, S. (2004). "A Simplified Method for Simulation of Strong Ground Motion Using Rupture Model of the Earthquake Source", Journal of Seismology, Vol. 8, No. 4, pp. 467–484.
22. Joshi, A., Singh, S. and Giroti, K. (2001). "The Simulation of Ground Motions Using Envelope Summations", Pure and Applied Geophysics, Vol. 158, No. 5-6, pp. 877–902.
23. Keilis-Borok, V.I. (1959). "On the Estimation of the Displacement in an Earthquake Source and of Source Dimensions", Annali di Geofisica, Vol. XII, No. 2, pp. 205–214.
24. Kumar, N., Parvez, I.A. and Virk, H.S. (2005). "Estimation of Coda Wave Attenuation for NW Himalayan Region Using Local Earthquakes", Physics of the Earth and Planetary Interiors, Vol. 151, No. 3-4, pp. 243–258.
25. Kvamme, L.B. and Havskov, J. (1989). "Q in Southern Norway", Bulletin of the Seismological Society of America, Vol. 79, No. 5, pp. 1575–1588.
26. Lanczos, C. (1961). "Linear Differential Operators", D. Van Nostrand Co., London, United Kingdom.
27. Lee, W.H.K. and Lahr, J.C. (1972). "HYPO71: A Computer Program for Determining Hypocenter, Magnitude, and First Motion Pattern of Local Earthquakes", Open File Report, United States Geological Survey, Denver, U.S.A.
28. Mandal, P. and Rastogi, B.K. (1998). "A Frequency-Dependent Relation of Coda Q_c for Koyna Warna Region, India", Pure and Applied Geophysics, Vol. 153, No. 1, pp. 163–178.
29. Mandal, P., Pandhy, S., Rastogi, B.K., Satyanarayana, V.S., Kousalya, M., Vijayraghavan, R. and Srinivasan, A. (2001). "Aftershock Activity and Frequency-Dependent Low Q_c in the Epicentral Region of 1999 Chamoli Earthquake of M_W 6.4", Pure and Applied Geophysics, Vol. 158, No. 9-10, pp. 1719–1736.
30. Paul, A., Gupta, S.C. and Pant, C.C. (2003). "Coda Q Estimates for Kumaun Himalaya", Proceedings of the Indian Academy of Sciences (Earth and Planetary Sciences), Vol. 112, No. 4, pp. 569–576.
31. Pelton, J.R. (2005). "Near-Surface Seismology: Wave Propagation" in "Near Surface Geophysics (edited by D.K. Butler)", Society of Exploration Geophysicists, Tulsa, U.S.A.
32. Press, W.H., Teukolsky, S.A., Vetterling, W.T. and Flannery, B.P. (1992). "Numerical Recipes", Cambridge University Press, New York, U.S.A.

33. Pujades, L.G., Canas, J.A., Egozcue, J.J., Puigvi, M.A., Gallart, J., Lana, X., Pous, J., Casas, A. (1990). "Coda Q Distribution in the Iberian Peninsula", Geophysical Journal International, Vol. 100, No. 2, pp. 285–301.
34. Rhea, S. (1984). "Q Determined from Local Earthquakes in the South Carolina Coastal Plain", Bulletin of the Seismological Society of America, Vol. 74, No. 6, pp. 2257–2268.
35. Rodriguez, M., Havskov, J. and Singh, S.K. (1983). "Q from Coda Waves Near Petatlan, Guerrero, Mexico", Bulletin of the Seismological Society of America, Vol. 73, No. 1, pp. 321–326.
36. Roecker, S.W., Tucker, B., King, J. and Hartzfeld, D. (1982). "Estimates of Q in Central Asia as a Function of Frequency and Depth Using the Coda of Locally Recorded Earthquakes", Bulletin of the Seismological Society of America, Vol. 72, No. 1, pp. 129–149.
37. Rovelli, A. (1984). "Seismic Q for Lithosphere of Montenegro Region (Yugoslavia): Frequency, Depth and Time Windowing Effects", Physics of the Earth and Planetary Interiors, Vol. 34, No. 3, pp. 159–172.
38. Sato, H. and Fehler, M.C. (1997). "Seismic Wave Propagation and Scattering in the Heterogeneous Earth", Springer Verlag, Berlin, Germany.
39. Shakal, A.F., Huang, M.-J. and Graizer, V.M. (2004). "California: Strong Motion Instrumentation Program Record Processing Methods and Procedures" in "Proceedings of Invited Workshop on Strong Motion Record Processing (edited by D.M. Boore, B.S.-J. Chiou, W.D. Iwan, D.R. O'Connell, A.F. Shakal, J.C. Stepp and C.M. Johnson)", COSMOS Publication CP-2004/02, Richmond, U.S.A.
40. Sharma, M.L. and Wason, H.R. (1994). "Occurrence of Low Stress Drop Earthquakes in the Garhwal Himalaya Region", Physics of the Earth and Planetary Interiors, Vol. 85, No. 3-4, pp. 265–272.
41. Singh, S.K., Iglesias, A., Dattatrayam, R.S., Bansal, B.K., Rai, S.S., Perez-Campos, X., Suresh, G., Baidya, P.R. and Gautam, J.L. (2006). "Muzaffarabad Earthquake of 8 October 2005 (M_W 7.6): A Preliminary Report on Source Characteristics and Recorded Ground Motions", Current Science, Vol. 91, No. 5, pp. 689–695.
42. Sipkin, S.A. and Jordan, T.H. (1979). "Frequency Dependence of Q_{ScS}", Bulletin of the Seismological Society of America, Vol. 69, No. 4, pp. 1055–1079.
43. Toksöz, M.N., Johnston, D.H. and Timur, A. (1979). "Attenuation of Seismic Waves in Dry and Saturated Rocks—I. Laboratory Measurements", Geophysics, Vol. 44, No. 4, pp. 681–690.
44. Trifunac, M.D. (1977). "Uniformly Processed Strong Motion Earthquake Ground Accelerations in the Western United States of America for Period from 1933 to 1971: Pseudo Relative Velocity Spectra and Processing Noise", Report USC/CE-77-04, University of Southern California, Los Angeles, U.S.A.
45. Valdiya, K.S. (1999). "Fast Uplift and Geomorphic Development of the Western Himalaya" in "Geodynamics of the NW Himalaya (edited by A.K. Jain and R.M. Manickvasgam)", Gondwana Research Group Memoir No. 6, Field Science, Osaka, Japan.
46. van der Baan, M. (2002). "Constant Q and a Fractal Stratified Earth", Pure and Applied Geophysics, Vol. 159, No. 7-8, pp. 1707–1718.
47. Yang, X., Lay, T., Xie, X.B. and Thorne, M.S. (2007). "Geometric Spreading of P_n and S_n in a Spherical Earth Model", Bulletin of the Seismological Society of America, Vol. 97, No. 6, pp. 2053–2065.
48. Zeng, Y., Anderson, J.G. and Yu, G. (1994). "A Composite Source Model for Computing Realistic Synthetic Strong Ground Motions", Geophysical Research Letters, Vol. 21, No. 8, pp. 725–728.